



Defect-Mediated Room Temperature Ferromagnetism in Lead-Free Ferroelectric $\text{Na}_{0.5}\text{Bi}_{0.5}\text{TiO}_3$ Materials

D. D. Dung¹ · N. Q. Dung² · N. B. Doan^{3,4} · N. H. Linh¹ · L. H. Bac¹ · N. N. Trung¹ · N. V. Duc⁵ · L.T. H. Thanh¹ · L. V. Cuong⁴ · D. V. Thiet¹ · S. Cho⁶

Received: 19 October 2019 / Accepted: 12 December 2019 / Published online: 4 January 2020
© Springer Science+Business Media, LLC, part of Springer Nature 2020

Abstract

The injection of ferromagnetism properties to ferroelectric materials is a feasible strategy for integrating new functionalities to create next-generation electronic devices. In this study, Ni-doped lead-free ferroelectric $\text{Na}_{0.5}\text{Bi}_{0.5}\text{TiO}_3$ materials were synthesized using the sol-gel method. The optical band gap was reduced from 3.12 eV to 2.23 eV for un-doped and 9 mol% Ni-doped $\text{Na}_{0.5}\text{Bi}_{0.5}\text{TiO}_3$ materials, respectively, when Ni was substituted at the Ti site. The Ni-doped $\text{Na}_{0.5}\text{Bi}_{0.5}\text{TiO}_3$ materials exhibited ferromagnetism at room temperature. The maximum magnetization was found to be $0.91 \mu_B/\text{Ni}$. Our work offers insight into the role of transition metals in room temperature ferromagnetism in lead-free ferroelectric materials for the creation of new types of green multiferroic materials.

Keywords $\text{Na}_{0.5}\text{Bi}_{0.5}\text{TiO}_3$ · Sol-gel · Ferromagnetic · Lead-free ferroelectric

PACS numbers 75.30.Hx · 75.85.+t · 77.84.Dy · 75.50.Pp

1 Introduction

The multiferroic materials are promised to create the next-generation electronic devices because their materials exhibited both magnetic and ferroelectric in one material, and moreover that external electrical field could control the magnetization

together with external magnetic field and could tune the electrical polarization [1, 2]. The research aimed to overcome the limited number of multiferroic materials that exist in nature which were well explained by Hill et al. [3, 4]. They explained that the scarcity of observed multiferroic materials in perovskite structures is due to the typical atomic-level mechanism, which prevents the simultaneous occurrence of ferroelectric and ferromagnetic conditions [3, 4]. In addition, the ferromagnetic state is usually ordered at below room temperature, hindering the application of devices that operate above room temperature [5]. Therefore, obtaining multiferroic materials above room temperature remains a challenge.

Among the current multiferroic materials, doping transition metals into ferroelectric materials is one of the simple ways to obtain ferromagnetism at room temperature, because of the oxygen vacancies and/or the exchange splitting among spin sub-bands through the crystal field of transition metals [6–10]. In fact, the various transition metals (Fe-, Mn-, Ni-) doped PbTiO_3 materials were successfully fabricated which exhibited the room temperature ferromagnetism [8–10]. In addition, the other ways to archive the room temperature ferromagnetism with strong magnetoelectric coupling were obtained in ferroelectric-ferromagnetic composites or multilayer thin film [11–13]. The main disadvantage of lead-based ferroelectric

✉ D. D. Dung
dung.dangduc@hust.edu.vn

¹ School of Engineering Physics, Hanoi University of Science and Technology, 1 Dai Co Viet road, Hanoi, Vietnam
² Department of Chemistry, Thai Nguyen University of Education, 20 Luong Ngoc Quyen Street, Thai Nguyen, Vietnam
³ CNRS, Institut Néel, F-38042 Grenoble, France and Univ. Grenoble Alpes, Institut Néel, F-38042 Grenoble, France
⁴ Faculty of Engineering Physics and Nanotechnology, University of Engineering and Technology, Vietnam National University, Building E3, 144 Xuan Thuy, Cau Giay, Hanoi, Vietnam
⁵ School of Electronics and Telecommunications, Hanoi University of Science and Technology, 1 Dai Co Viet road, Hanoi, Vietnam
⁶ Department of Physics, University of Ulsan, Ulsan 680-749, Republic of Korea

PbTiO₃ materials is its high lead content (60 wt%), which is harmful to the environment and the human. Nevertheless, the recent research still concentrated on the Pb-based materials due to their excellent electronic properties, and many equipment used the electronic part containing lead element [14]. Thus, the integration of the room temperature ferromagnetism in current lead-based ferroelectric materials has saved investment costs and expanded the function materials for application in smart electronic devices. Recently, the developed countries have issued the prohibition of the use of lead-based materials in the electronic device [15].

In recent years, there has been an increasing interest in the two lead-free perovskites (Na_{0.5}Bi_{0.5}TiO₃ and K_{0.5}Bi_{0.5}TiO₃) due to the strong ferroelectric properties, such as a large polarization and a low coercive field which are comparable to that of lead-based ferroelectric materials [16]. Therefore, induction room temperature ferromagnetism in lead-free ferroelectric Bi-based materials is really promised to replace the Pb-based in electronic devices. The ion metal doped in K_{0.5}Bi_{0.5}TiO₃ ceramics can be split on the spin under crystal field of K_{0.5}Bi_{0.5}TiO₃. Recently, the ferromagnetism at room temperature in Fe-doped K_{0.5}Bi_{0.5}TiO₃ ceramics was explained by spin splitting of transition metal ions under crystal field [6]. The room temperature ferromagnetism was also obtained in Ni-doped K_{0.5}Bi_{0.5}TiO₃ materials which resulted from intrinsic and contribution from extrinsic as clusters [7]. Previous studies have reported that magnetic moment contributed by Ni ions as doping in K_{0.5}Bi_{0.5}TiO₃ materials was larger than that of contribution of magnetic spin at high-spin state [7]. However, the ferromagnetism in Co-doped Na_{0.5}Bi_{0.5}TiO₃ materials at room temperature was suggested to originate from Co clusters because of reduction oxidation state of Co during fabrication [17]. The ferromagnetism at room temperature in case of Fe-doped Na_{0.5}Bi_{0.5}TiO₃ ceramics contributed by intrinsic phenomenon due to the competition between diamagnetism and ferromagnetism as Fe dopants was low, while the competition between paramagnetic-like and ferromagnetic behavior was observed at high Fe concentration dopants [18]. Recently, the weak ferromagnetism at room temperature was obtained for Cr-doped Bi_{0.5}Na_{0.5}TiO₃ materials which possibly resulted from oxygen vacancies [19]. Eventually, the current integration of room temperature ferromagnetic properties in lead-free ferroelectric materials has some good potential properties, but the origin of interaction of transition metal to favor magnetic ordering was still debated, especially in the transition metal, which has multivalence states.

In this study, the Ni-doped Na_{0.5}Bi_{0.5}TiO₃ materials were fabricated using the sol-gel method. The optical band gap values (E_g) were reduced from 3.12 eV to 2.23 eV as the Ni concentration was increased to 9 mol%. A weak ferromagnetism was observed in un-doped Na_{0.5}Bi_{0.5}TiO₃ because of the trade-off between diamagnetism and ferromagnetism.

Comparable ferromagnetism and paramagnetism were obtained in Ni-doped Na_{0.5}Bi_{0.5}TiO₃ samples because of the Ni substitution at the Ti site. The magnetic moment saturation was found at approximately 0.91 μ_B /Ni at 5 K.

2 Experiment

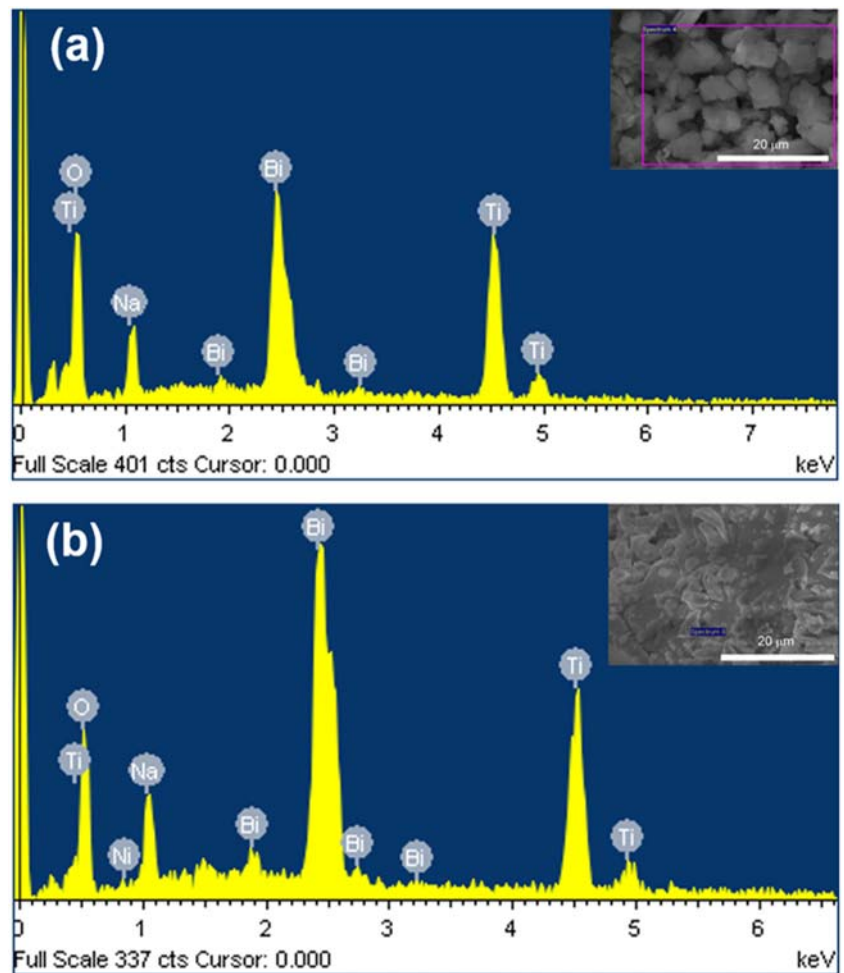
The un-doped Na_{0.5}Bi_{0.5}TiO₃ (i.e., NBT) and Ni-doped Na_{0.5}Bi_{0.5}TiO₃ (i.e., NBT-*x*Ni, where *x* = 0.5, 1, 3, 5, 7, and 9) samples were synthesized using the sol-gel method. The bismuth nitrate pentahydrate (Bi(NO₃)₂·5H₂O), sodium nitrate (NaNO₃), and nickel nitrate (Ni(NO₃)₂·6H₂O) were analytical grade. Firstly, they were dissolved in distilled water and acetic acid to make a clear solution. Then the acetylacetone and tetraisopropoxytitanium(IV) (C₁₂H₂₈O₄Ti) were added into the solution. The solutions were stirred at room temperature until it became transparent. Then, the dry gels were prepared by heating the sol at 100 °C. These gels were ground and sintered at 900 °C for 3 h. Sodium was added to the excess at approximately 20 mol% to prevent sodium loss during the gel and sintering processes. The compositions of the samples were varied by electron probe microanalysis (EPMA). The energy-dispersive X-ray spectroscopy (EDX) was used to detect the existence of elements in synthesized materials. The particle morphology and particle size were investigated by field emission scanning electron microscopy (FE-SEM). The crystal structures were analyzed by X-ray diffraction (XRD). The vibrational modes of the synthesized samples were studied by Raman spectroscopy. The optical properties of powders were characterized by UV–Vis spectroscopy. The magnetic properties were investigated by a superconducting quantum interference device (SQUID) magnetometer at 5 K and a vibrating-sample magnetometer (VSM) at room temperature.

3 Results and Discussion

Figure 1(a) and (b) shows the EDX spectra of pure Bi_{0.5}Na_{0.5}TiO₃ and 5 mol% Ni-doped Bi_{0.5}Na_{0.5}TiO₃ samples, respectively. The inset of each EDX spectrum was the selected area of samples for characterization. The EDX spectrum presented in Fig. 1(a) showed that all elements including Bi, Na, Ti, and O existed in the synthesized materials. The addition of Ni element together with base of pure Bi_{0.5}Na_{0.5}TiO₃ element for 5 mol% Ni-doped Bi_{0.5}Na_{0.5}TiO₃ as shown in Fig. 1 (b). In other words, the appearance of Ni elements was provided that the impurities of Ni element existed in doped samples.

The FE-SEM images of Ni-doped BNT with different molar ratios are shown in Fig. 2 (b)–(h). It is observed that the different molar ratios of Ni dopant show the same morphology in each case. The particles in pure BNT sample had a cubic-

Fig. 1 The EDX spectra of (a) pure $\text{Bi}_{0.5}\text{Na}_{0.5}\text{TiO}_3$ and (b) 5 mol% Ni-doped $\text{Bi}_{0.5}\text{Na}_{0.5}\text{TiO}_3$ samples. The inset of each figure was the selected area of samples for characterization



like shape. The particle size of BNT pure sample was less than that of Ni-doped sample. However, the particles in pure sample were strongly sintered together. The Ni-doped BNT samples had big particles with irregular shape.

The XRD patterns of un-doped and Ni-doped $\text{Na}_{0.5}\text{Bi}_{0.5}\text{TiO}_3$ samples were illustrated in Fig. 3(a). All diffraction peaks and their relative intensities were matched to the JCPDS standard data of the $\text{Na}_{0.5}\text{Bi}_{0.5}\text{TiO}_3$ materials. The

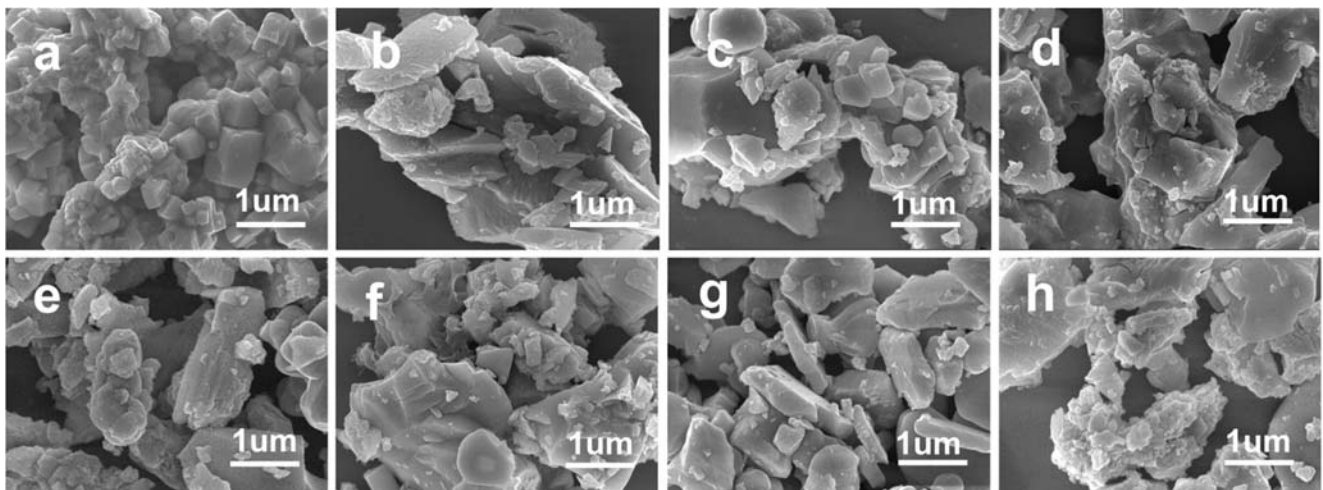


Fig. 2 The FE-SEM image of $\text{Bi}_{0.5}\text{Na}_{0.5}\text{TiO}_3$ ceramics with different Ni concentrations: (a) pure BNT, (b) 0.5 mol%, (c) 1 mol%, (d) 2 mol%, (e) 3 mol%, (f) 5 mol%, (g) 7 mol%, and (h) 9 mol%

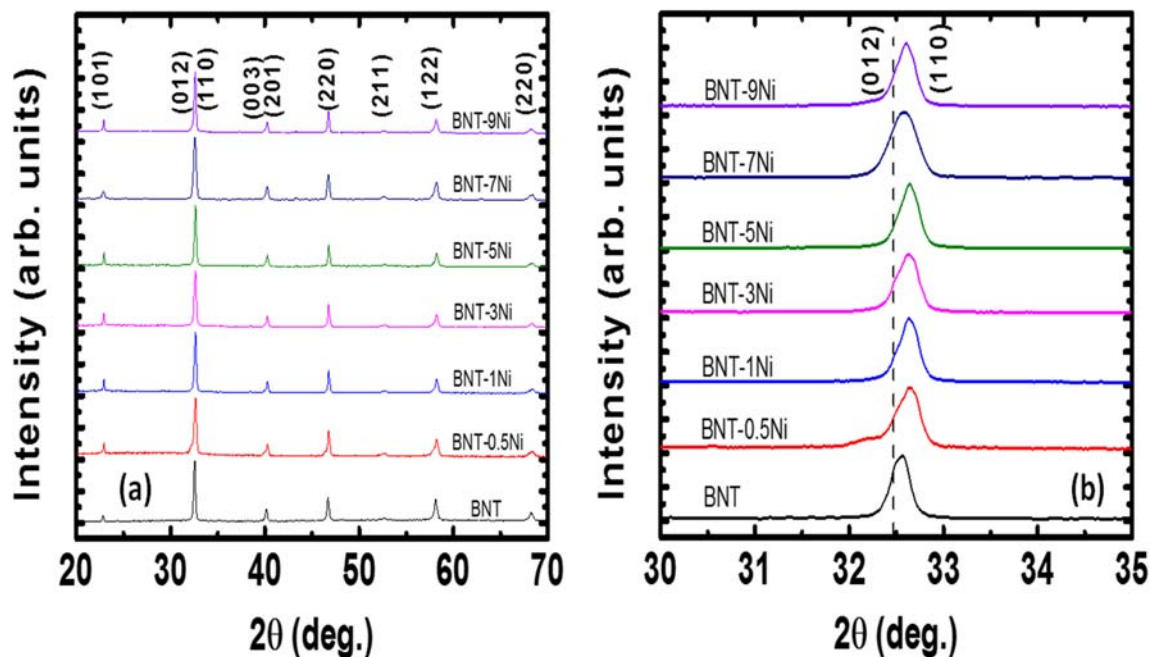


Fig. 3 (a) XRD patterns of un-doped and Ni-doped $\text{Na}_{0.5}\text{Bi}_{0.5}\text{TiO}_3$ samples with different Ni-doping concentrations; (b) comparison of (012) diffraction peak positions

impurity phase could not be detected in the XRD pattern. Comparison of the location of (012) diffraction peaks in the range of 30° – 35° shows that the position of the peaks of the Ni-doped samples slightly shifted to higher 2θ values, as plotted in Fig. 3(b). The distorted structure indicates that Ni was incorporated with the lattice structure and compressed the lattice parameters. The ionic radii of Ni^{2+} , Ni^{3+} , Ni^{4+} , and Ti^{4+} with six coordination are 0.069, 0.056, 0.048, and 0.061 nm, respectively [20]. Therefore, the Ni^{2+} cations substitution for Ti^{4+} cations resulted in expansion of lattice parameter, while replacement of Ti^{4+} by Ni^{3+} or Ni^{4+} cations resulted in compression of the lattice parameter. The valence state of Ni cations was dependent on the host materials and chemical environment around the Ni cations. Lebedev et al. reported that the oxidation state of Ni in $\text{Ba}_{1-x}\text{Sr}_x\text{TiO}_3$ compound changes from Ni^{4+} in SrTiO_3 to $\text{Ni}^{2.5+}$ in BaTiO_3 when x was varied and the changing of Ni states originated from different formation energies of the oxygen vacancies in these compounds [21]. In addition, Sluchinskaya et al. pointed out that the mean Ni charge states are around $\text{Ni}^{2.5+}$ where Ni^{2+} ions are in a high-spin state at the B-sites of the ABO_3 perovskite structure, and the difference of charges of Ni^{2+} and Ti^{4+} is mainly compensated by distant oxygen vacancies [22]. XAF spectroscopy analysis studied Ni-doped SrTiO_3 provided that the oxidation state of Ni is close to $4+$ [23]. As a result of the multivalence state of Ni cations, the optical absorbance spectroscopy of Ni-doped $\text{K}_{0.5}\text{Bi}_{0.5}\text{TiO}_3$ had multi-absorbance peaks [7]. Therefore, it is difficult to determine the main reason for the distorted structure due to the multivalence state of Ni ions in the samples [22–26]. In addition, oxygen vacancies created by

the unbalanced state of $\text{Ni}^{2+/3+}$ with Ti^{4+} can also affect the lattice structure [24]. In other words, the distorted structure of $\text{Na}_{0.5}\text{Bi}_{0.5}\text{TiO}_3$ materials provided the evidence for incorporation of Ni cation into host lattice.

Figure 4(a) shows the Raman spectra of un-doped $\text{Na}_{0.5}\text{Bi}_{0.5}\text{TiO}_3$ and Ni-doped $\text{Na}_{0.5}\text{Bi}_{0.5}\text{TiO}_3$ samples in the wave number range of 150 – 1000 cm^{-1} . Un-doped $\text{Na}_{0.5}\text{Bi}_{0.5}\text{TiO}_3$ samples have relatively broad Raman bands because of the disorder at the A-site and the overlapping Raman modes. The shape of Raman scattering spectra of Ni-doped $\text{Na}_{0.5}\text{Bi}_{0.5}\text{TiO}_3$ samples was shown in similar which provide the maintainable structure of $\text{Na}_{0.5}\text{Bi}_{0.5}\text{TiO}_3$ samples. The broad vibration modes resulted in difficulty to distinguish each vibration modes. For $\text{Na}_{0.5}\text{Bi}_{0.5}\text{TiO}_3$ Raman band, the modes in the frequency range from 155 cm^{-1} to 187 cm^{-1} and from 246 cm^{-1} to 401 cm^{-1} were dominated by Na–O and TiO_6 vibrations, respectively, while the higher-frequency modes in the range from 413 cm^{-1} to 826 cm^{-1} were primarily associated with oxygen atom vibrations [27]. The effect of Ni substitution for Ti on the phonon vibration is shown in Fig. 4(b), in which the high magnification Raman spectra of un-doped and Ni-doped $\text{Na}_{0.5}\text{Bi}_{0.5}\text{TiO}_3$ were in the wave number range from 200 cm^{-1} to 400 cm^{-1} . The results indicate that the Ti–O bands shifted to a lower frequency as the amount of Ni dopants increased, further proving the Ni substitution at the Ti site as a possible result from the higher mass of the Ni ions ($\sim 58.71\text{ g/mol}$) than that of the Ti ions ($\sim 47.90\text{ g/mol}$).

Figure 5(a) shows the optical absorption spectra of un-doped $\text{Na}_{0.5}\text{Bi}_{0.5}\text{TiO}_3$ and Ni-doped $\text{Na}_{0.5}\text{Bi}_{0.5}\text{TiO}_3$ samples with various Ni concentrations. The results were clearly

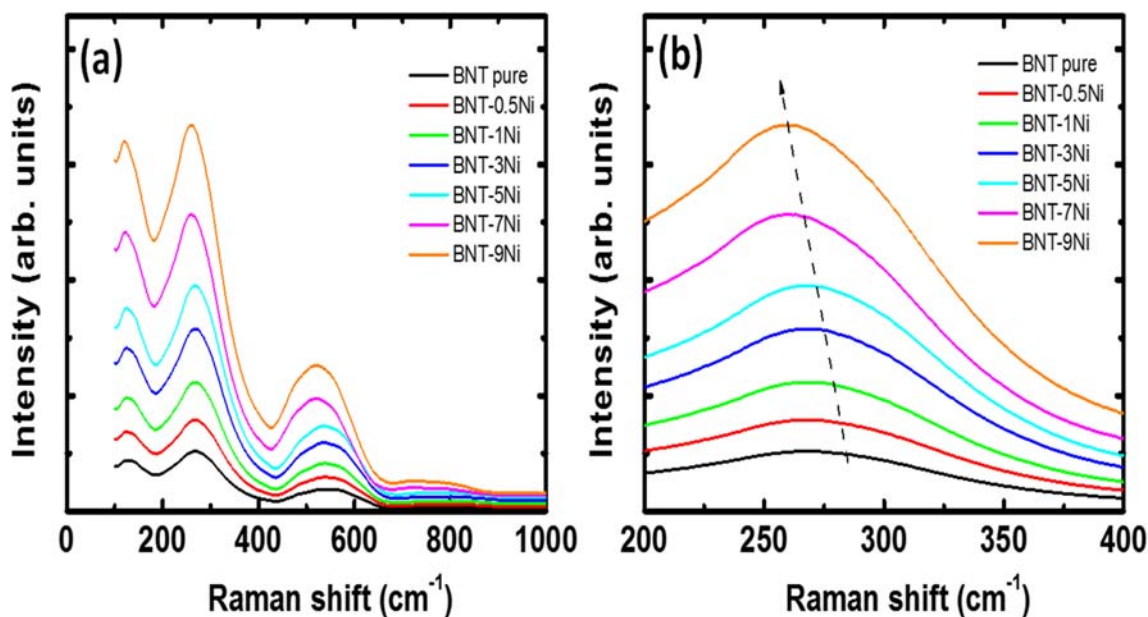


Fig. 4 (a) Raman spectra of the un-doped $\text{Na}_{0.5}\text{Bi}_{0.5}\text{TiO}_3$ and Ni-doped $\text{Na}_{0.5}\text{Bi}_{0.5}\text{TiO}_3$ samples as a function of Ni doping concentration; and (b) magnification Raman spectra in the range of 200–400 cm^{-1} of the pure $\text{Na}_{0.5}\text{Bi}_{0.5}\text{TiO}_3$; and Ni-doped $\text{Na}_{0.5}\text{Bi}_{0.5}\text{TiO}_3$ samples

indicated that the absorption edge was red shift with increasing of Ni content. Consequently, the band gap (E_g) value was

decreased. These findings were more evident for Ni cations incorporated into the crystal structure of $\text{Na}_{0.5}\text{Bi}_{0.5}\text{TiO}_3$ and

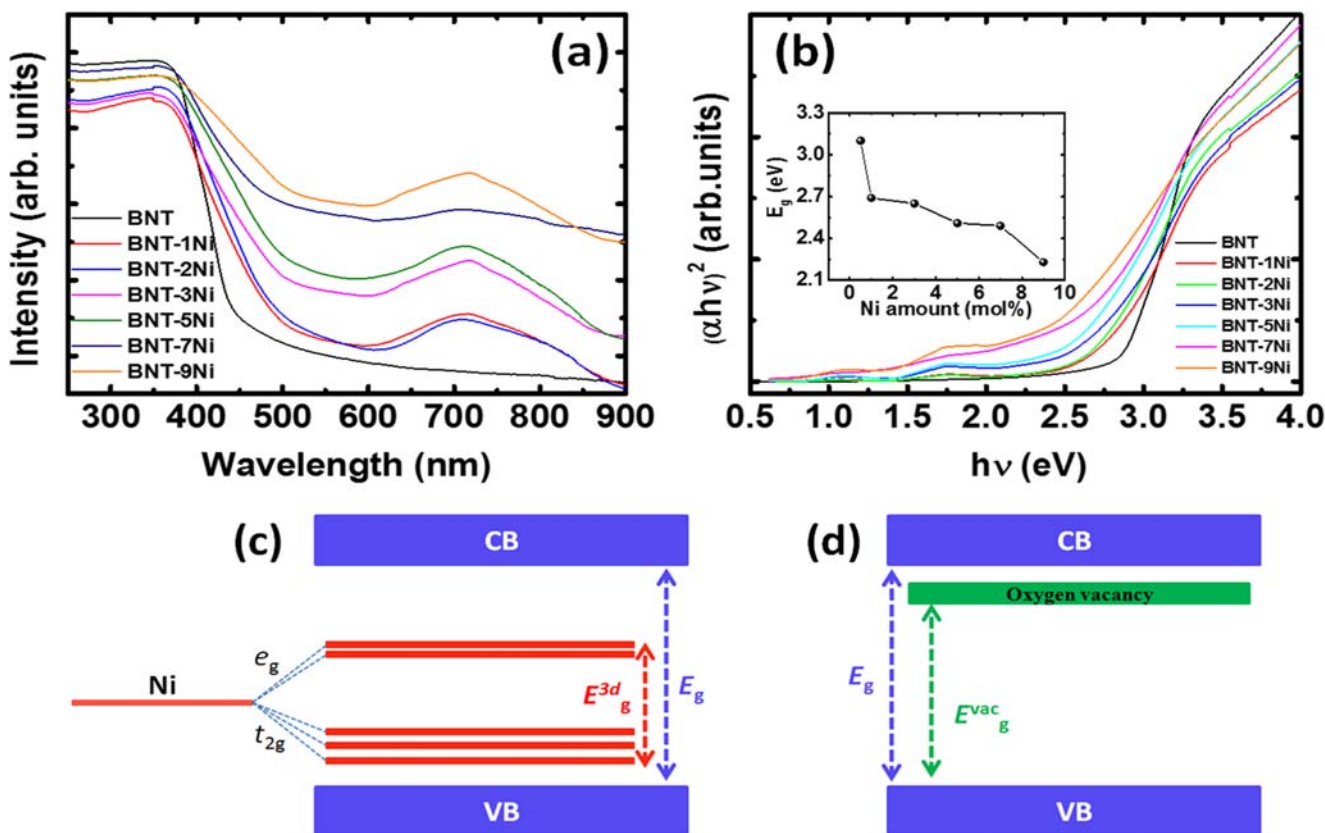


Fig. 5 (a) UV–Vis absorption spectra; (b) dependence of $(\alpha h\nu)^2$ on photon energy ($h\nu$) of the pure $\text{Na}_{0.5}\text{Bi}_{0.5}\text{TiO}_3$ and Ni-doped $\text{Na}_{0.5}\text{Bi}_{0.5}\text{TiO}_3$ samples with various concentrations. The inset of (b) shows the optical band gap values of the $\text{Na}_{0.5}\text{Bi}_{0.5}\text{TiO}_3$ samples as a

function of Ni dopant. The proposal reduction optical band gap energy of $\text{Na}_{0.5}\text{Bi}_{0.5}\text{TiO}_3$ materials from (c) transition metals and (d) oxygen vacancies

consequently changed the band structure. In addition, the appearance of a multi-absorbance peak in the range of 600–900 nm suggested the existence of multiple local states for Ni [7]. This result was obtained by complex observation using XRD spectroscopy, as discussed above. The E_g values were evaluated using Tauc method as plotted in Fig. 5(b). The optical band gap was calculated as 3.12 eV for un-doped $\text{Na}_{0.5}\text{Bi}_{0.5}\text{TiO}_3$ samples, and this value decreased to 2.23 eV for 9 mol% Ni-doped $\text{Na}_{0.5}\text{Bi}_{0.5}\text{TiO}_3$ samples. Figure 5(b) provides the details of E_g values as a function of the amount of Ni dopants. The values of E_g as a function of Ni concentration are illustrated in the inset of Fig. 5 (b). The results are consistent with recent published work that the band gap of lead-free ferroelectric $\text{K}_{0.5}\text{Bi}_{0.5}\text{TiO}_3$ ceramics is changed by substitution of Fe, Ni, or Mn at the Ti site [6, 7, 28]. Thus, we suggest that d -orbital electronics should be incorporated into the lattice by Ni ion doping to make the local electronic state which resulted in reducing the optical band gap of $\text{Na}_{0.5}\text{Bi}_{0.5}\text{TiO}_3$ materials. Furthermore, the origin of reduction on optical band gap in Ni-doped $\text{Na}_{0.5}\text{Bi}_{0.5}\text{TiO}_3$ samples is proposed in Fig. 5(c) and (d) for transition metal and oxygen vacancies, respectively. Under crystal field, the spin splitting in d electrons of transition metal ions creates the local state in middle band gap. Besides, oxygen vacancies were created due to unbalance charge of $\text{Ni}^{2+/3+}$ dopant Ti^{4+} host and/or promotion from surface defect or self-defect during fabrication, which normally locates near the conduction band.

Furthermore, the effect of d electrons on ferromagnetic properties of $\text{Na}_{0.5}\text{Bi}_{0.5}\text{TiO}_3$ samples was observed by determining the magnetic moment with respect to the magnetic field plot of un-doped and Ni-doped $\text{Na}_{0.5}\text{Bi}_{0.5}\text{TiO}_3$ samples, as shown in Fig. 6. Figure 6(a) shows the magnetic hysteresis (M – H) loops of the un-doped $\text{Na}_{0.5}\text{Bi}_{0.5}\text{TiO}_3$ and Ni-doped $\text{Na}_{0.5}\text{Bi}_{0.5}\text{TiO}_3$ samples at room temperature. A hysteresis loop with an anti- S shape can be observed, which directly results from the weak ferromagnetic and diamagnetic competition [6, 7, 17, 18]. By incorporating Ni in the $\text{Na}_{0.5}\text{Bi}_{0.5}\text{TiO}_3$ lattice, the diamagnetic signal converts to a ferromagnetic loop, thereby confirming ferromagnetism at a low magnetic field. In addition, the unsaturated shape in the M – H curves is obtained for Ni dopants with concentration of more than 5 mol% presumably because of the contribution of isolated Ni ions in the $\text{Na}_{0.5}\text{Bi}_{0.5}\text{TiO}_3$ host matrix [6, 7]. This phenomenon has been demonstrated for Fe- and Co-modified $\text{Na}_{0.5}\text{Bi}_{0.5}\text{TiO}_3$ ceramics [17, 18]. The remanent magnetization and coercive field are estimated to be approximately 90 Oe and 0.3 memu/g, respectively, both of which further demonstrating the room temperature ferromagnetism behavior. Those values consist of the recently reports for transition metal doped lead-free ferroelectric materials such as for Fe- and Ni-doped $\text{K}_{0.5}\text{Bi}_{0.5}\text{TiO}_3$ materials or Mn-doped $\text{Na}_{0.5}\text{Bi}_{0.5}\text{TiO}_3$ ceramics [6, 7, 29]. The results also perform with the observation of transition metal doped lead-based

ferroelectric material such as Mn-doped or Ni-doped PbTiO_3 materials [9, 10]. Figure 4(b) shows the dependence of the magnetization on the temperature under an applied field of 1 kOe of $\text{Na}_{0.5}\text{Bi}_{0.5}\text{Ti}_{0.99}\text{Ni}_{0.01}\text{O}_3$ samples. The inset of Fig. 6(b) shows the M – H curve of the $\text{Na}_{0.5}\text{Bi}_{0.5}\text{Ti}_{0.99}\text{Ni}_{0.01}\text{O}_3$ samples under a magnetism of up to 70 kOe at 5 K. The maximum magnetization is found to be ~ 0.241 emu/g corresponding to $0.91 \mu_B/\text{Ni}$ at 5 K. The value was smaller than that of Ni-doped $\text{K}_{0.5}\text{Bi}_{0.5}\text{TiO}_3$ materials where the observation of maximum magnetization was $3.44 \mu_B/\text{Ni}$ at 5 K [7].

Further understanding the observation ferromagnetism with low saturation of magnetic moment in case of Ni-doped $\text{Na}_{0.5}\text{Bi}_{0.5}\text{TiO}_3$ than that of Ni-doped $\text{K}_{0.5}\text{Bi}_{0.5}\text{TiO}_3$ materials, the possible spin configuration of Ni ions is drawn in Fig. 7. Note that Ni ions have three valence states of Ni^{2+} , Ni^{3+} , and Ni^{4+} state. Ni^{2+} and Ni^{4+} ions have low-spin state only while Ni^{3+} ions have been stable in both low- and high-spin state [20]. Thus, the possible schematic spin configurations of Ni^{2+} , Ni^{3+} , and Ni^{4+} ions are illustrated at Fig. 5(a)–(c), respectively. In the consideration of the spin-only magnetic moment, the magnetic moment of Ni^{2+} is $1 \mu_B/\text{Ni}$, and Ni^{3+} is $0.5 \mu_B/\text{Ni}$ and $1.5 \mu_B/\text{Ni}$ for low- and high-spin configuration, respectively, while the Ni^{4+} has no magnet moment. Our experimental results have provided that the magnetic moment of Ni is $0.91 \mu_B/\text{Ni}$ which is close with Ni^{2+} state as considering the contribution from spin only. The results also consisted with recent observation of divalent state of Ni ions in Ni-doped $\text{Na}_{0.5}\text{Bi}_{0.5}\text{TiO}_3$ materials [30]. Thus, it could be suggested that the original ferromagnetism in Ni-doped $\text{Na}_{0.5}\text{Bi}_{0.5}\text{TiO}_3$ majorly originated from low-spin state interaction of Ni ion in $\text{Bi}_{0.5}\text{Na}_{0.5}\text{TiO}_3$ materials.

Further understanding the origin of room temperature ferromagnetism in Ni-modified $\text{Na}_{0.5}\text{Bi}_{0.5}\text{TiO}_3$ materials, the first principle calculation was performed for materials by using density functional theory (DFT). The crystal structure of Ni-doped $\text{Na}_{0.5}\text{Bi}_{0.5}\text{TiO}_3$ materials is prepared by using the VESTA package, as presented in Fig. 8 [31]. All DFT calculations were carried out by PWScf code executed in Quantum-Espresso package [32]. The exchange-correlation energy was performed by the generalized gradient approximation (GGA) technique using Perdew–Burke–Ernzerhof (PBE) exchange-correlation functionals [33]. Plane-wave basis set cutoffs for the smooth part of wave functions and the augmented density were 45 Ry and 250 Ry, respectively. In order to reduce computational resources, pristine $\text{Na}_{0.5}\text{Bi}_{0.5}\text{TiO}_3$ (NBT) was simulated by the primitive cell of $R3c$ with 2 Bi/Na cation in Wyckoff symmetric position $2a$, 2 Ti cations in $2a$ and 6 O anions in $6a$ (Fig. 8) and the lattice constants from the experiments [34, 35]. A supercell of $2 \times 2 \times 2$ of doped $\text{Na}_{0.5}\text{Bi}_{0.5}\text{Ti}_{0.9375}\text{Ni}_{0.0625}\text{O}_3$ (NBTN) compounds with the doping concentration of 6.25% was created by replacing 1 Ti atom by a Fe atom in a supercell of $2 \times 2 \times 2$ of $\text{Na}_{0.5}\text{Bi}_{0.5}\text{TiO}_3$ to form the unit cell of NBTN. The Brillouin

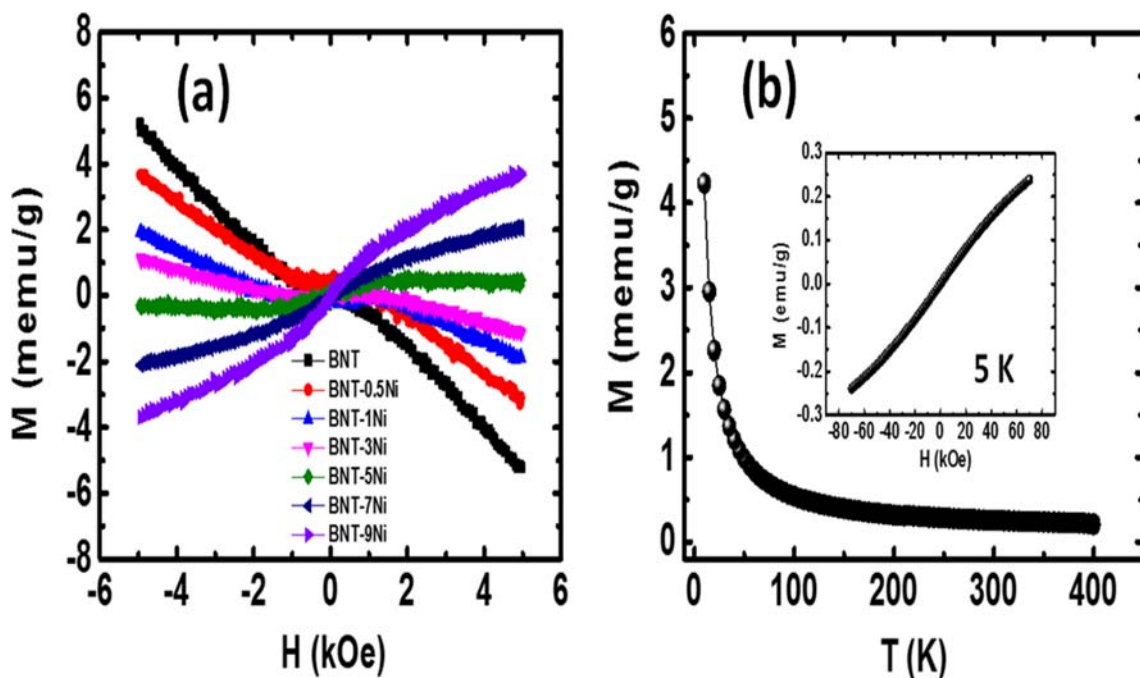


Fig. 6 (a) M – H curves of the un-doped $\text{Na}_{0.5}\text{Bi}_{0.5}\text{TiO}_3$ and Ni-doped $\text{Na}_{0.5}\text{Bi}_{0.5}\text{TiO}_3$ samples with various Ni amounts and (b) M – T curve at 1 kOe magnetic field for the Ni-doped $\text{Na}_{0.5}\text{Bi}_{0.5}\text{TiO}_3$ samples with

1 mol%. The inset of Fig. 6(b) shows the M – H curve of the 1 mol% Ni-doped $\text{Na}_{0.5}\text{Bi}_{0.5}\text{TiO}_3$ sample at 5 K

zone was sampled by the Monkhorst–Pack scheme [36]. The structures are totally relaxed with a mesh of $2 \times 2 \times 2$, and the mesh of k -space is raised to $4 \times 4 \times 4$ in the static and density of state (DOS) calculations.

Figure 9(a) and (b) shows the calculated PDOS of $\text{Na}_{0.5}\text{Bi}_{0.5}\text{TiO}_3$ and Ni-doped $\text{Na}_{0.5}\text{Bi}_{0.5}\text{TiO}_3$, respectively. The PDOS results of $\text{Na}_{0.5}\text{Ti}_{0.5}\text{O}_3$ materials were provided that the hybridization of Bi–O at energy range of -10 eV and the narrow band near Fermi level. It suggests for the influence of Bi on electronic structures of $\text{Na}_{0.5}\text{Bi}_{0.5}\text{TiO}_3$ -based materials, especially, the active states near Fermi level. The broad hybridization of Na–O shows at energy range from -8 eV to -2 eV, which

presents for the strong covalent bond between Na cation and O cation. As seen in Table 1, Ni cations gain more electrons and broaden the band in PDOS. Meanwhile, Bi cations lose electrons and become more positive. It makes the interaction between Bi and O more ionic than covalent in NBTN. However, the light hybridization of Bi–O near Fermi level, which present for the covalent bond of Bi–O, induces a little spin polarization in PDOS of Bi near Fermi level. While BNT is completely spin-unpolarized, BNNT shows slightly the spin polarization, which is mostly due to the contribution of PDOS of Ti and Ni in NBTNs. Mostly, interactions between B -site cations and O anions in BO_6 octahedrons of perovskite structure are more ionic

Fig. 7 The spin configuration of Ni ions in octahedral site of $\text{Na}_{0.5}\text{Bi}_{0.5}\text{TiO}_3$ materials (a) Ni^{2+} ions, (b) Ni^{3+} ions, and (c) Ni^{4+} ions

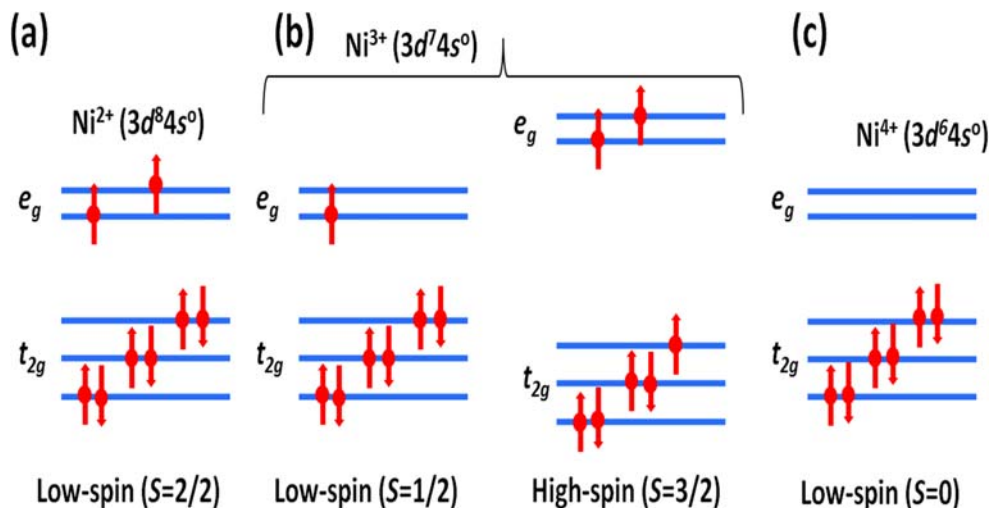
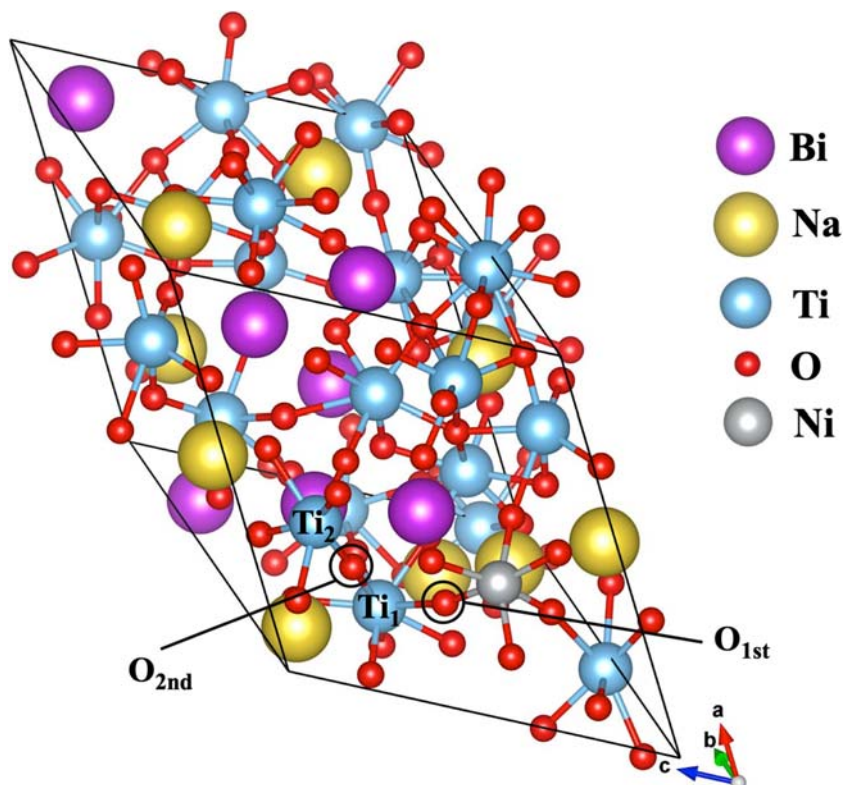


Fig. 8 Rhombohedral supercell of $2 \times 2 \times 2$ is established from rhombohedral primitive cell of NBT. Purple, yellow, blue, red, and silver cycles are represented for Bi, Na, Ti, O, and doping Ni in NBT. Ti_1 and Ti_2 are denoted for Ti ions of first nearest neighbor and the second nearest neighbor octahedral TiO_6 of transition metal doping position, viz., Ti_{1st} and Ti_{2nd} . O_{1st} and O_{2nd} are twofold-coordinated bridge O between $Ni-Ti_{1st}$ and $Ti_{1st}-Ti_{2nd}$. Crystal structure is prepared by using the VESTA package [31]



than covalent. However, in these materials, the interaction between *B*-site cations and O anions seems to be more complicated.

Figure 10 provides a detail view of the interaction between *B*-site cations and O anion. In NBTN, $3d$ electrons

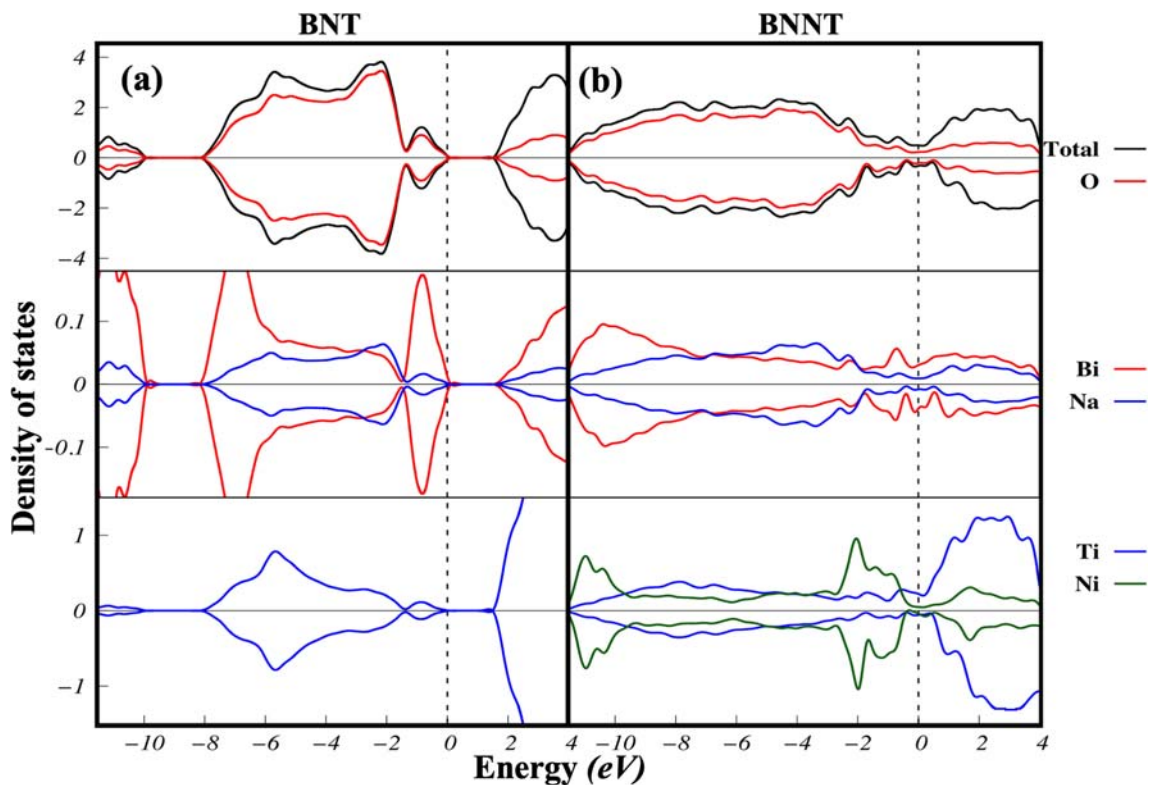


Fig. 9 Calculated projected density of states (PDOS) of cations (Bi, Na, Ti, and Ni) and anion O of (a) NBT and (b) NBTN compounds. Zero corresponds to Fermi energy (E_F)

Table 1 Charge ($\pm\Delta Q$) gain/loss by Bi, Na, O_{1st}, O_{2nd}, Ti_{1st}, and Ti_{2nd} due to doping Ni into pristine NBT compounds to form NBTN compounds. Plus/negative signs are represented for gaining/losing charge, respectively. And, magnetic moment of Ni, O_{1st}, Ti_{1st}, O_{2nd}, and Ti_{2nd} in NBTN

Charge (e)	ΔQ_{Bi}	ΔQ_{Na}	$\Delta Q_{\text{O}_{1\text{st}}}$	$\Delta Q_{\text{O}_{2\text{nd}}}$	$\Delta Q_{\text{Ti}_{1\text{st}}}$	$\Delta Q_{\text{Ti}_{2\text{nd}}}$
	-0.51	0.46	0.36	-0.04	0.15	0.14
Magnetic moment (μ_{B})	μ_{Ni}	$\mu_{\text{O}_{1\text{st}}}$	$\mu_{\text{Ti}_{1\text{st}}}$	$\mu_{\text{O}_{2\text{nd}}}$	$\mu_{\text{Ti}_{2\text{nd}}}$	
	0.01	0.02	0.24	~0.00	0.28	

of Ni predominantly distribute in d_{xy} and $d_{x^2+y^2}$ orbitals and strongly localize in the energy range from -2 eV to -0.5 eV. However, these d electrons do not have the hybridization with p orbital of the nearest O cation, i.e., O_{1st} p orbital. It means that the interactions between Ni cation and surrounding O cations are more ionic than covalent. As a result, Ni cation and O_{1st} cations seem to be slightly spin-polarized. Doping Ni into pristine Na_{0.5}Bi_{0.5}TiO₃ compounds induces charge gain in Ti_{1st} and Ti_{2nd} ions as seen in Table 1 and increases the states near to Fermi level in PDOS of Ti_{1st} and Ti_{2nd} ions. This increase prompts the spin polarization in Ti_{1st} and Ti_{2nd} ions.

Consequently, electronic structure of NBTN leads to the magnetic moments of Ni, O_{1st}, O_{2nd}, Ti_{1st}, and Ti_{2nd} ions in NBTN, which are presented in Table 1. While Ni ion exhibits the small magnetic moment (0.01 μ_{B}), Ti_{1st} and Ti_{2nd} ions establish the relative magnetic moment of 0.24 μ_{B} and 0.28 μ_{B} . Thus, the magnetic behavior of Ni-doped Na_{0.5}Bi_{0.5}TiO₃ ceramics was most relative with low-spin state of Ni cation, and the magnetic moment was contributed from Ti nearest cause of charge transfer. However, the effect of Ti and O vacancies and also the presence of Ni with different valence states also needed to be further investigated.

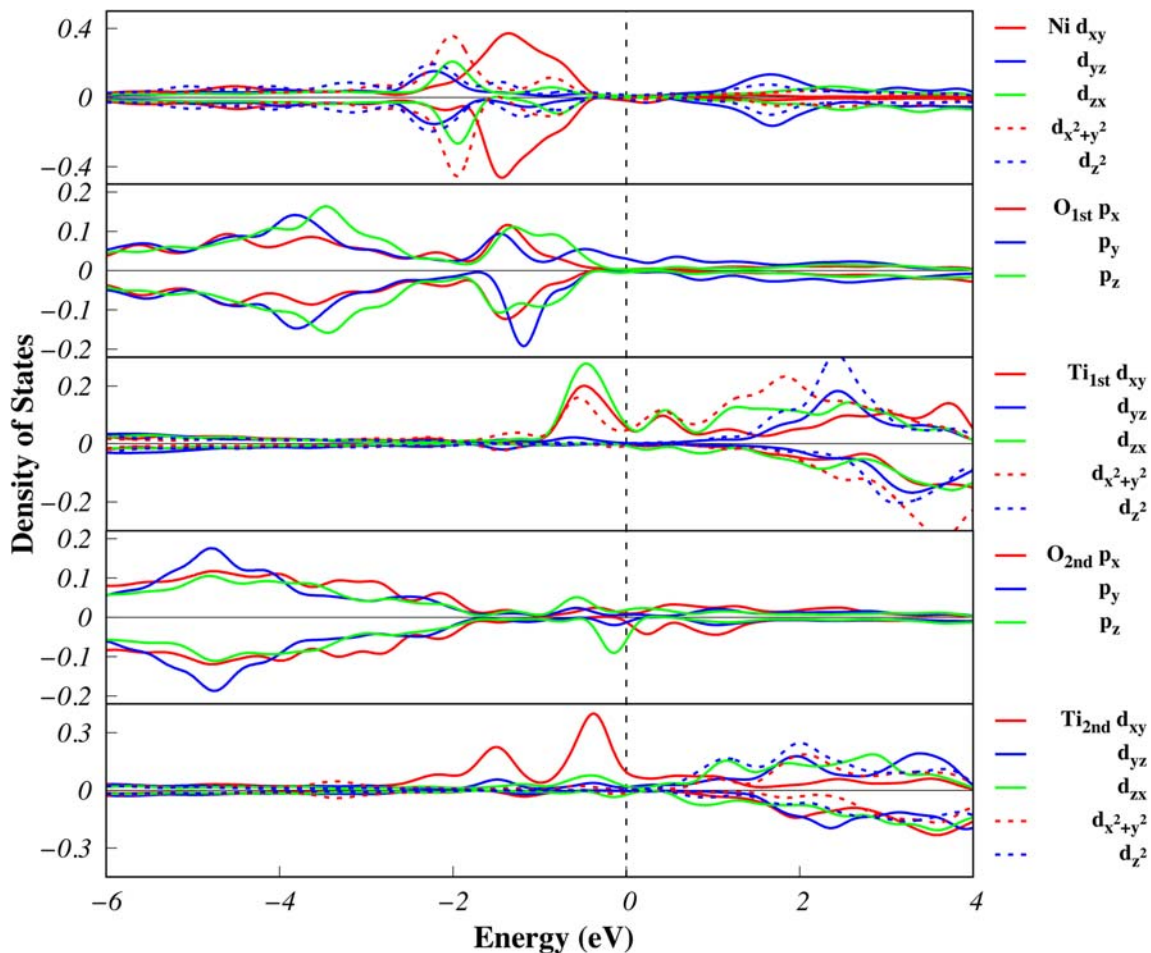


Fig. 10 Calculated PDOS of specific position sites in NBTN compounds, i.e., O_{1st}, Ti_{1st}, O_{2nd}, Ti_{2nd} ions, and the doping Ni. Ti_{1st} and Ti_{2nd} are denoted for Ti cations of the nearest and next nearest TiO₆ octahedrons to

doping Ni position. O_{1st} and O_{2nd} are denoted for the twofold-coordinated O ion which are the bridge bonds between Ni and Ti_{1st} and Ti_{2nd}, respectively. Zero corresponds to Fermi energy (E_F)

4 Conclusion

Room temperature ferromagnetism was achieved in un-doped and Ni-doped $\text{Na}_{0.5}\text{Bi}_{0.5}\text{TiO}_3$ materials. Optical band gap values decreased from 3.12 eV for un-doped $\text{Na}_{0.5}\text{Bi}_{0.5}\text{TiO}_3$ to 2.23 eV for 9 mol% Ni-doped $\text{Na}_{0.5}\text{Bi}_{0.5}\text{TiO}_3$. The unsaturated shape of ferromagnetic M – H curves could be observed with the concentration of more than 5 mol% Ni-doped $\text{Na}_{0.5}\text{Bi}_{0.5}\text{TiO}_3$ compounds due to the contribution of isolated $3d$ transition ions at Ti sites. The maximum magnetization was found to be $0.91 \mu_{\text{B}}/\text{Ni}$. This study offers insight into the integration of transition metals into ferroelectric materials to develop new types of multiferroic materials based on lead-free ferroelectric materials.

Acknowledgments This research is funded by the Hanoi University of Science and Technology (HUST) under project number T2018-TD-201.

References

- Junquera, J.: *Physic.* **9**, 28 (2016)
- Wang, H., Wen, J., Miller, D.J., Zhou, Q., Chen, M., Lee, H.N., Rabe, K.M., Wu, X.: *Phys. Rev. X.* **6**, 011027 (2016)
- Hill, N.A., Filippetti, A.: *J. Magn. Magn. Mater.* **242–245**, 976–979 (2002)
- Hill, N.A.: *J. Phys. Chem. B.* **104**, 6694–6709 (2000)
- Scott, J.F., Blinc, R.: *J. Phys. Condens. Mater.* **23**, 1132202 (2011)
- Dung, D.D., Thiet, D.V., Odkhuu, D., Cuong, L.V., Tuan, N.H., Cho, S.: *Mater. Lett.* **156**, 129–133 (2015)
- Thiet, D.V., Cuong, D.D., Bac, L.H., Cuong, L.V., Khoa, H.D., Cho, S., Tuan, N.H., Dung, D.D.: *Mater. Trans.* **56**, 1339–1343 (2015)
- Ren, Z., Xu, G., Wei, X., Liu, Y., Hou, X., Du, P., Weng, W., Shen, G., Han, G.: *Appl. Phys. Lett.* **91**, 063106 (2007)
- Oanh, L.M., Do, D.B., Phu, N.D., Mai, N.T.P., Minh, N.V.: *IEEE Trans. Magn.* **50**, 2502004 (2014)
- Oanh, L.M., Do, D.B., Minh, N.V.: *Mater. Trans.* **56**, 1358–1361 (2015)
- Wang, B.Y., Wang, H.T., Singh, S.B., et al.: *RSC Adv.* **3**, 7884–7893 (2013)
- Murakami, M., Chang, K.S., Aronova, M.A., Lin, C.L., Yu, M.H., Simpers, J.H., Wuttig, M., Takeuchi, I.: *Appl. Phys. Lett.* **87**, 112901 (2005)
- Cherepov, S., Amiri, P.K., Alzate, J.G., Wong, J., Lewis, M., Upadhyaya, P., Nath, J., Bao, M., Bur, A., Wu, T., Carman, G.P., Khitun, A., Wang, K.L.: *Appl. Phys. Lett.* **104**, 082403 (2014)
- Jo, W., Dittmer, R., Acosta, M., Zang, J., Groh, C., Sapper, E., Wang, K., Rodel, J.: *J. Electroceram.* **29**, 71–93 (2012)
- Li, Y., Moon, K.S., Wong, C.O.: *Science.* **380**, 1419–1420 (2005)
- Quan, N.D., Bac, L.H., Thiet, D.V., Hung, V.N., Dung, D.D.: *Adv. Mater. Sci. Eng.* **2014**, 365391 (2014)
- Wang, Y., Xu, G., Ji, X., Ren, Z., Weng, W., Du, P.: *J. Alloys Compd.* **475**, L25–L30 (2009)
- Wang, Y., Xu, G., Yang, L., Ren, Z., Wei, X., Weng, W.: *Mater. Sci.* **27**, 471–476 (2009)
- Thanh, L.T.H., Doan, N.B., Dung, N.Q., Cuong, L.V., Bac, L.H., Duc, N.A., Bao, P.Q., Dung, D.D.: *J. Electron. Mater.* **46**, 3367–3372 (2017)
- Shannon, R.D.: *Acta Crystallogr. A.* **32**, 751–767 (1976)
- Lebedev, A.I., Sluchinskaya, I.A.: *Ferroelectrics.* **501**, 1–8 (2016)
- Sluchinskaya, I.A., Lebedev, A.I.: *Phys. Solid State.* **59**, 1512–1519 (2017)
- Sluchinskaya, I.A., Lebedev, A.I., Erko, A.: *J. Adv. Dielect.* **03**, 1350031 (2013)
- Das, S.K., Mishra, R.N., Roul, B.K.: *Solid State Commun.* **191**, 19–24 (2014)
- Niishiro, R., Kato, H., Kudo, A.: *Phys. Chem. Chem. Phys.* **7**, 2241–2245 (2005)
- Shah, J., Kotnala, R.K.: *J. Mater. Chem. A.* **1**, 8601 (2013)
- Niranjan, M.K., Karthik, T., Asthana, S., Pan, J., Waghmare, U.V.: *J. Appl. Phys.* **113**, 194106 (2013)
- Tuan, N.H., Thiet, D.V., Odkhuu, D., Bac, L.H., Binh, P.V., Dung, D.D.: *Physica B Condens. Mater.* **532**, 108–114 (2018)
- Thanh, L.T.H., Doan, N.B., Bac, L.H., Thiet, D.V., Cho, S., Bao, P.Q., Dung, D.D.: *Mater. Lett.* **186**, 239–242 (2017)
- Pradhan, S.K., De, S.K.: *Ceram. Int.* **44**, 15181–15191 (2018)
- Momma, K., Izumi, F.: *J. Appl. Crystallogr.* **44**, 1272–1276 (2011)
- Giannozzi, P., Baroni, S., Bonini, N., et al.: *J. Phys. Condens. Matter.* **21**, 395502 (2009)
- Perdew, J.P., Burke, K., Ernzerhof, M.: *Phys. Rev. Lett.* **77**, 3865 (1996)
- Jones, G.O., Thomas, P.A.: *Acta Crystallogr. Sect. B: Struct. Sci.* **58**, 2168 (2002)
- Jones, G.O., Kreisel, J., Jennings, V., Geday, M.A., Thomas, P.A.: *Ferroelectrics.* **270**, 191 (2002)
- Monkhorst, H.J., Pack, J.D.: *Phys. Rev. B.* **13**, 5188 (1976)

Publisher's Note Springer Nature remains neutral with regard to jurisdictional claims in published maps and institutional affiliations.